Liquid-liquid dispersion in co-current disc and doughnut pulsed column : effect of the operating conditions, physical properties and materials parameters

Emeline Lobry, Christophe Gourdon, Catherine Xuereb, Thierry Lasuye

Liquid–liquid dispersion in co-current disc and doughnut pulsed column effect of the operating conditions, physical properties and materials parameters

Emeline Lobry [a,*], Christophe Gourdon [a], Catherine Xuereb [a], Thierry Lasuye [b]

[a] Université de Toulouse, INPT, UPS, CNRS, Laboratoire de Génie Chimique (LGC), 4, Allée Emile Monso, BP 84234, 31030 Toulouse Cedex 4, France
[b] SAV, Usine de Mazingarbe, BP49, 62160 Bully Les Mines, France

HIGHLIGHTS

- Co-current disc and doughnut pulsed column.
- High volume dispersed phase fraction.
- Effect of hydrodynamic and materials.
- Modelling through dimensionless number.

Keywords:
Liquid–liquid dispersion
Pulsed column in co-current flow
Concentrated emulsion

ABSTRACT

Pulsed columns are traditionally used to perform liquid–liquid extractions at counter-current. They are currently seen as a potential tubular reactor to perform co-current continuous processes. In this paper the case of liquid–liquid dispersion is considered. Various parameters are investigated such as the dispersed phase holdup, the flowrate and pulsation conditions but also some process parameters such as the packing material or the physical properties such as the type of surfactant. The energy dissipation rate is estimated according to correlations found in literature. Breakage and coalescence rate models are applied in order to understand the various observed phenomena. Finally, a correlation to predict the mean droplet size is proposed depending on various dimensionless numbers characterizing the flow, the internal and the physico-chemistry of the phase systems.

1. Introduction

Among the available continuous technologies, the pulsed column has already been largely studied in the past, mainly for counter-current liquid–liquid extraction processes [1]. It consists in a column packed with discs and doughnuts equally spaced or perforated sieved plates.

Today, this kind of tubular plug flow reactors could be used for continuous crystallization, for polymerization [2,3] or for biodiesel production [4] but with a co-current flow.

In this paper, we focus on the liquid–liquid dispersion mechanism which supports various processes, most of the time batch-wise. A lot of processes require a control of the initial mean droplet size and droplet size distribution to provide the correct properties of the final product.

Moreover, in order to avoid the solvent removal and to increase productivity, it is interesting to produce liquid–liquid dispersion at a high dispersed phase fraction. Indeed, it is expected to decrease the cost, but also to facilitate the separation steps in order to obtain the final product and to reduce the effluent post-treatment operations.

Nowadays, the industry is interested in developing continuous processes to replace the classical batch reactors. In stirred tanks the emulsification duration is generally the time needed to reach stabilized mean droplets sizes. This characteristic duration ranges from few minutes to hours [5–9].

Continuous processes can significantly reduce this duration which corresponds to the residence time. Besides, continuous processes offer a higher level of control on the different process parameters such as droplet size and exhibit plug flow behavior. They also enhance temperature management compared to batch process. Calabrese and Pissavini [10] present the benefits of continuous processes in terms of cost, safety and quality.

The study of various designs in literature confirms the ability of pulsed flows to perform a good mixing [11,12] and transport of liquid–liquid dispersion and liquid–solid suspension [13]. The continuous oscillatory baffled reactor (COBR, Nitech®), a special

* Corresponding author. Tel.: +33 (0)5 34 32 36 72.
E-mail address: emeline.lobry@ensiacet.fr (E. Lobry).

design composed of rings equally spaced has been extensively studied. Heat transfer [14], mixing performance [15,16], and liquid–liquid dispersion [17–19] have been particularly detailed but often in batch process.

In this paper, our goal is to study the performance of a co-current pulsed upflow disc and doughnut column performing a liquid–liquid dispersion with a controlled mean diameter. Two model systems are investigated: Water/PVA/Toluene and Water/SDS/Toluene. PVA is partially hydrolyzed polyvinyl acetate and SDS is sodium dodecyl sulphate. The aim of this study is to analyze the effect of the operating conditions (pulsation and flowrate), design parameters (material) and physical properties (surfactant and dispersed phase holdup) on mean droplet size and on the droplet size distribution. Identification of the relevant parameters affecting the liquid–liquid dispersion characteristics (droplets size distributions, mean droplets size, etc.) leads to propose a correlation to predict the Sauter mean drop diameter.

2. Materials and methods

2.1. Fluids used

In this study two water/oil/surfactant systems are investigated varying only by the surfactant type (anionic or non ionic). Toluene (95%) was purchased from Gaches Chimie. PVA is partially hydrolyzed polyvinyl acetate and is a non ionic surfactant. It was provided by Nippon Gohsei. Sodium dodecyl sulphate (SDS) was provided by Panreac and is an anionic surfactant. The liquid–liquid dispersion created consists in oil in water (O/W) dispersion.

The properties of the different systems are summarized in Table 1. The interfacial tension is measured by the pendant drop method (Krüss DSA 100). Viscosity measurements are carried out using an AR 2000 rheometer (TA Instruments).

The aqueous phase is composed of distilled water and surfactant and the dispersed phase is only composed of toluene.

2.2. Experimental rig

The experimental set up consists of a 3 m long column of 50 mm internal diameter D_c packed with immobile discs and doughnuts equally alternated and spaced ($H = 24$ mm) made of stainless steel (316 L) or PTFE. The inner diameter of the ring aperture is D_a and the disc diameter is D_d. Both diameters are fitted in order to obtain the same transparency factor T (ratio between inserts area to cross section) for the disc or the doughnuts. The characteristics of the different inserts (disc and doughnut) are given in Fig. 1. Whatever the insert's materials, the open free area T (transparency factor) is of 26%. They are mounted horizontally and centered with respect to the column axis. One level represents either two doughnuts (or rings) separated by a disc or two discs separated by a doughnut (Fig. 1). The outer edge of the rings is extended to the column wall. The flow follows two routes: a central one through the ring aperture and a peripheral one between the disc edge and the column wall.

Table 1
Physicochemical properties of the two systems.

	Water/PVA/toluene	Water/SDS/toluene
ρ_c (kg m^{-3})	997	998
ρ_d (kg m^{-3})	870	870
μ_c (Pa s)	0.0059	0.0059
μ_d (Pa s)	0.001	0.001
Surfactant concentration	0.07% mass/kg toluene	2.3% mass/kg toluene
σ_e (mN m^{-1})	3.5	3.5

The aqueous phase is prepared in a 220 L tank in which the water and the surfactant are mixed. The toluene is stored in a 200 L tank. Each tank is under constant weighting to check the flowrates. The two flows are pumped through membrane pumps to the bottom of the column. The feed lines are equipped with anti-pulsatory balloons which absorb the pulsation due to the volumetric pumps and then ensure a constant flowrate. The pulsation is imposed via a pump without check valves allowing the control of the oscillation amplitude, A, via the pump vernier and of the oscillation frequency f, thanks to the variable frequency regulator. This device induces reciprocal up and down movements of the fluids inside the column. Different samples are collected all along the column: at the basis (generation of the dispersion at the first doughnuts) and after every stage to measure the droplet size distribution.

The amplitude A describes the total displacement of the flow. In our case, the minimum amplitude is equal to the length between a disc and a doughnut $H_{\min}$ and the maximum amplitude to the difference between two discs or two doughnuts, $H_{\max}$.

The dispersed phase holdup in volume Φ (hold-up) is defined thanks to the respective phases flowrates as follows:

$$\Phi = \frac{Q_d}{Q_d + Q_c} = \frac{Q_d}{Q_{tot}} \quad (1)$$

where Q_d, Q_c and Q_{tot} are respectively the dispersed phase, continuous phase and total volume flowrates.

It implicitly suggests that there is no slip velocity.

2.3. Analytical aspects

2.3.1. Interfacial tension measurement

Due to the presence of surfactants in the aqueous phase, the interfacial tension between the toluene and the aqueous phase evolves dynamically until it reaches its equilibrium value. In a continuous process, the interfacial tension evolves all along the equipment due to the constant breakup-coalescence processes and the rearrangement of the surfactant molecules at the interface. In both studied systems, the surfactant concentration in the aqueous phase is above the critical micellar concentration (concentration mentioned in Table 1).

The transient interfacial tension is measured for each system via the pendant drop method (Krüss DSA100). It consists in generating a drop at a tip of a needle. A CCD camera allows the recording of the drop shape. Then, thanks to the droplet image analysis software, the interfacial tension is calculated via the Young–Laplace equation. The method is well-known and has been largely commented in different publications [20].

2.3.2. Contact angle measurement

At the inserts surface, three phases are in contact. As previously described, a first interface composed by the two liquid phases is created: the dispersed phase and the continuous phase containing the surfactant. The internal represents the third phase (solid). Depending on the internal type (made of stainless steel or PTFE), it is expected that the liquid phases interact differently resulting in different behaviors of the phase systems.

To analyze the interaction, the contact angle of a single drop is measured via the Krüss DSA100 by using the captive bubble method.

A piece of the internal is maintained in the aqueous phase and thanks to a curved needle, a toluene droplet is posed on the surface. The complementary part of the contact angle is then measured. The inserts used for measurement are part of the column inserts. Table 2 reports the values of the different contact angles.

As it was expected, stainless steel surface is more hydrophilic than the PTFE internal. It seems that the PTFE is not preferentially

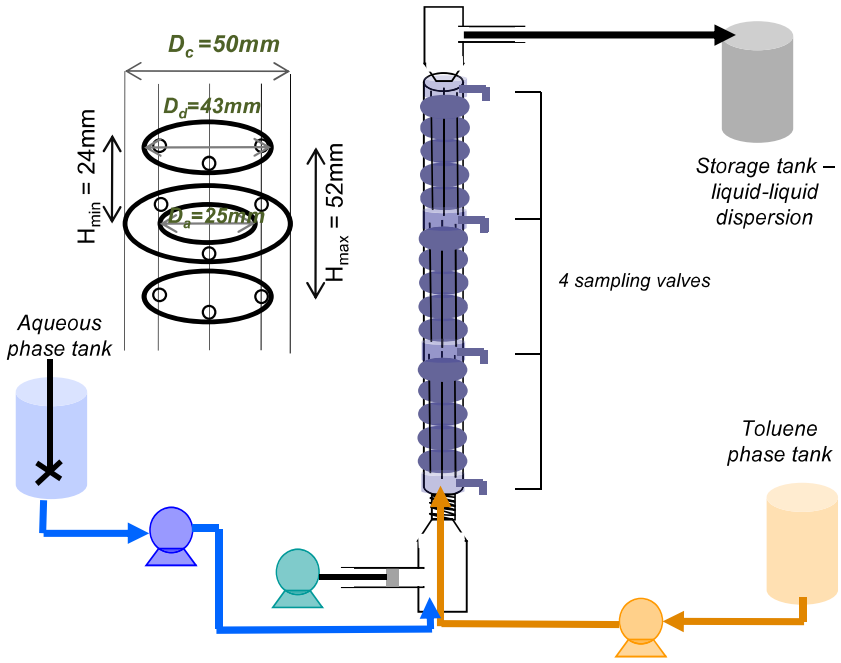

Fig. 1. Experimental rig of the disc and doughnut pulsed column.

Table 2
Contact angle measurement via the Krüss DSA100.

	PTFE	Stainless steel
Contact angle between solid/toluene droplet in aqueous phase (PVA + water) (°)	55.2	121.8
Contact angle between aqueous phase and solid in air (°)	92.1	43.5
Contact angle between solid/toluene droplet in aqueous phase (SDS + water) (°)	79.1	

wetted by the aqueous phase. The behavior of stainless steel in our case can be considered as partially hydrophilic.

2.3.3. Droplet size measurements

The Mastersizer 2000 laser granulometer is based on the laser diffraction principle, and is frequently used for droplets size distributions analysis. It can measure droplet sizes from 0.02 to 2000 µm. The droplets pass through a focus laser beam. The light is scattered at an angle which is inversely proportional to the droplet size. The angular intensity is then measured by a series of photosensitive detectors. It is based on the Mie diffraction theory. The droplet size distribution is then calculated (volumetric percentage).

It provides information about the distribution characteristics such as different characteristic diameters and distribution width.

For future discussions, the mean Sauter diameters d_{32} (2) and the span which quantifies the width of the distribution (3) are defined:

$$d_{32} = \frac{\sum_{i=1}^{n} n_i d_i^3}{\sum_{i=1}^{n} n_i d_i^2} \quad (2)$$

where n_i is the number of droplets which sizes range from d_i to d_{i+1}.

$$\text{span} = \frac{d_{90} - d_{10}}{d_{50}} \quad (3)$$

The d_{90}, d_{10} represent respectively the highest diameter of 90% in volume of the dispersed phase and the highest diameter of 10% in volume of the dispersed phase, while d_{50} is the median diameter of the distribution, i.e. the highest diameter of 50% in volume of the dispersed phase. These characteristic diameters are directly derived from the laser diffraction analyses.

3. Preliminary studies

3.1. Emulsions stability

The two tested water/surfactant/toluene systems exhibit a creaming phenomenon which starts only a few minutes after emulsification. To check if this phenomenon is reversible, droplets size distributions obtained through laser diffraction analysis several minutes after the sampling and nearly 24 h after are compared (Fig. 2). The superimposition reveals that no irreversible behavior such as coalescence [21] or Ostwald ripening [22,23] occurs.

Same results are obtained for both systems which are quite stable during at least 24 h.

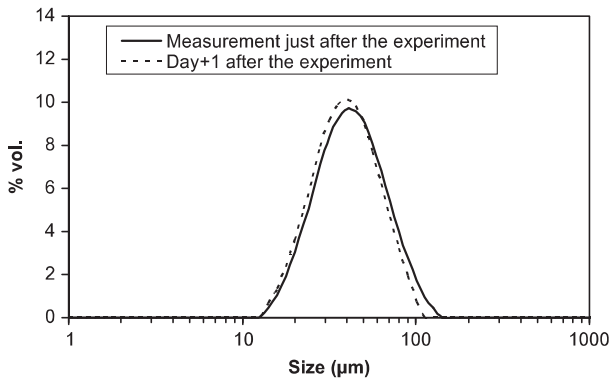

Fig. 2. Comparison of two droplet size distribution a few minutes after the sampling and 24 h after. Q_{tot} = 85 L h^{-1}, A = 52 mm, f = 1.56 Hz, H = 1 m, Φ = 25%, 3 m of PTFE packing.

3.2. Interfacial tension evolution along the column

Fig. 3a and b represents the interfacial tension evolution for both systems within the residence time range and until the pseudo equilibrium value.

The same interfacial tension equilibrium value is reached for both systems (Table 1). However, the surfactant is expected to adsorb faster using SDS rather than PVA. Indeed, the global kinetics of surfactant adsorption consists of three steps: the diffusion of the molecule at the interface, the adsorption of this molecule and finally the conformation arrangement of these molecules at the interface. Depending on the concentration and on the chemical nature of surfactants, each one of these steps can control the global kinetics of the surfactant adsorption.

Concerning the PVA, two different evolution zones can be identified. First, the interfacial tension decreases faster. This step corresponds to the diffusion and adsorption of PVA at the interface. Then the decreasing slows down. It refers to a rearrangement of the absorbed molecules at the interface [24–26]. On the contrary with SDS, the adsorption is extremely fast and the equilibrium is almost instantaneously reached.

In Fig. 3, the residence time range of the experiments (according to the flowrates) is indicated. The global adsorption kinetics of both surfactants is quite different: in case of SDS, the interfacial tension does not evolve significantly on the range studied and the value is close to the equilibrium value σ_e. Yet, with experiments involving PVA, the interfacial tension still decreases and the value is almost divided by an order of magnitude of two all along the column.

Values of the interfacial tension along the column are reported in the inserts in Fig. 3a and b. In case of SDS, the equilibrium value is almost obtained within the first meter while it is still evolving in the case of PVA surfactant, and the equilibrium value is not even reached at the higher flowrates.

3.3. Droplet size analysis

Fig. 4 exhibit the droplet sizes in the case of the water/PVA/toluene system. Fig. 4a represents the evolution of the mean Sauter diameter (defined by expression 2) at the different sample points. Fig. 4b, which is an optical microscopy picture taken after sampling, confirms that the emulsion is oil in water type with spherical droplets.

Moreover droplet size distributions are monomodal for all laser diffraction analyses of the whole samplings as observed in Fig. 2.

The stabilities of the droplet size distribution and of the mean droplet size all along the column have been studied. The degree of overlapping of the droplets size distribution is evaluated with respect to the column length of the system under various operating conditions.

Fig. 4a shows that the mean droplet size is maintained on the first 2 m and then tends to be larger along the column after 2 m of packing for different pulsation conditions.

The smallest droplets are created at the basis of the column whereas they become larger when they go up. In fact, the pulsation is not homogeneously distributed all along the column. Besides, the last sample point is located at the down comer where the

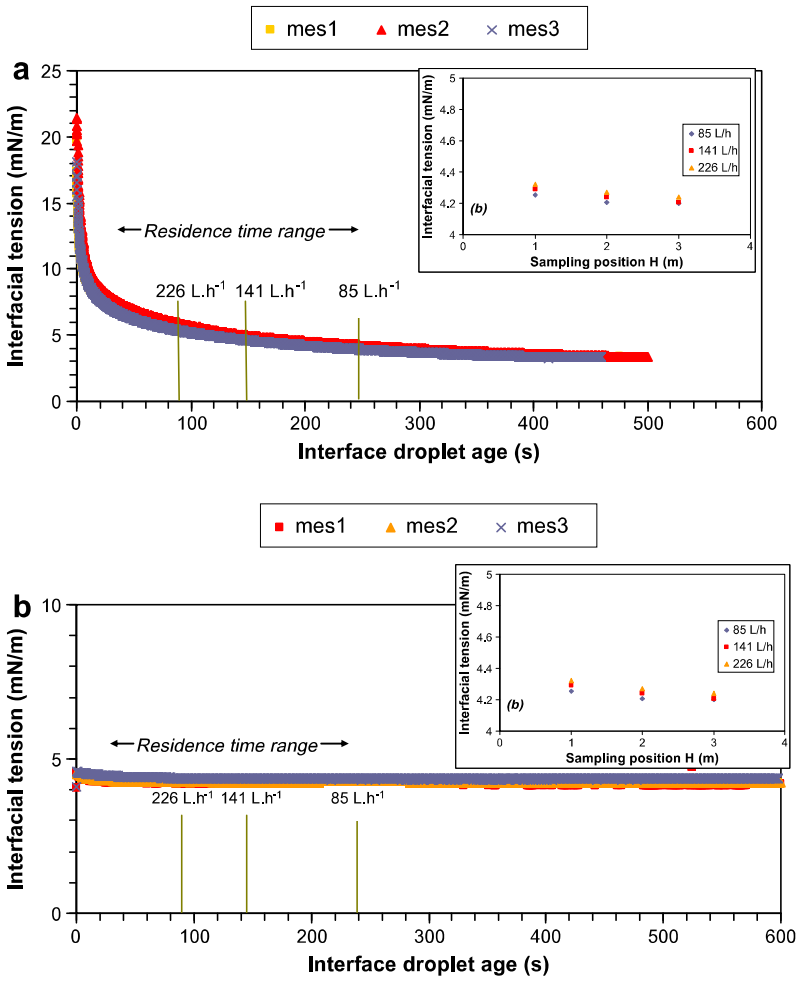

Fig. 3. Dynamic interfacial tension values for the (a) water/PVA/toluene and (b) water/SDS/toluene systems and values corresponding to the residence time in the column.

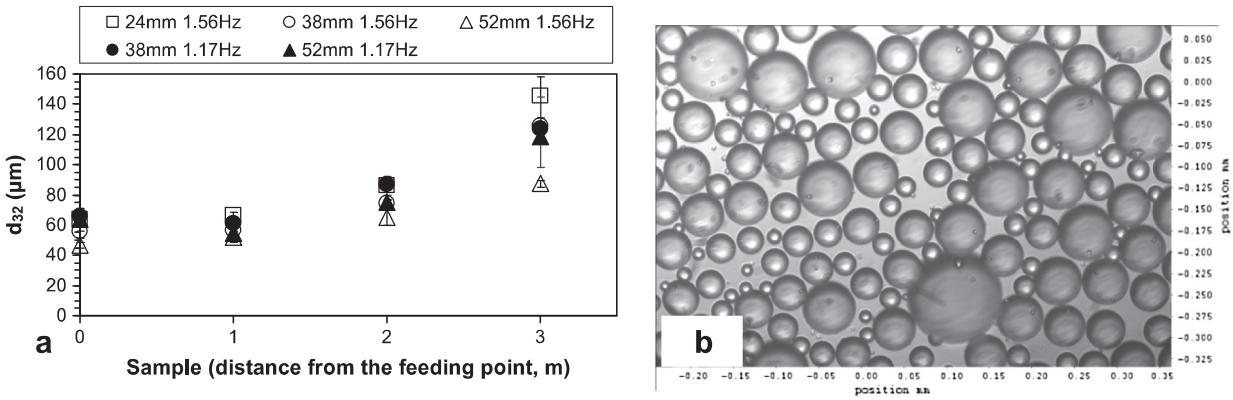

Fig. 4. Mean droplet size along the column for different pulsation conditions(a) and microscopic observation (b) of the Water/PVA/toluene dispersion obtained for Q_{tot} = 85 L h^{-1}, A = 38 mm, f = 1.56 Hz, Φ = 0.25, sample after 2 m for the picture with antipulsatory PTFE packing.

section is enlarged, leading to a decrease of the drop velocity. Consequently, the measurement is not taken into account for the following discussion.

4. Experimental results and discussion

In this section, the effect of the different parameters is investigated: throughput, pulsation conditions (amplitude, frequency), nature of surfactant, dispersed phase hold-up, internal (material, height).

4.1. Operating conditions

Operating conditions tested for the two systems are summed up in Table 3. The process conditions (flowrate and pulsation) are studied for both systems involving different surfactants. The material of the insert acts on the droplet size and droplet size distribution significantly. Consequently, the effect of the height of the insert and their nature on the liquid–liquid dispersion properties is investigated. The location of the dispersed phase feed line is also a studied parameter.

In this part the dimensionless numbers describing the pulsatile flow are defined.

The pulsatile flow contains a steady component and a superimposed periodical time varying component, called oscillation. Subsequently, the instantaneous velocity of the liquid in the column comprises also two components: a permanent one due to the flowrate U_0 and a pulsed one due to the pulsation $U_p(t)$, so that:

$$U(t) = U_0 + U_p(t) \tag{4}$$

The instantaneous pulsation velocity created by a piston mechanical device is given by:

$$U_p(t) = \pi A f \cos(2\pi f t) \tag{5}$$

where A and f are respectively the oscillation amplitude and frequency.

The mean flow velocity U_m is the sum of the permanent flow velocity U_0 and of the mean pulsation velocity U_{pm}, over a period T of oscillation, given by:

$$U_{pm} = \frac{1}{T}\int_0^T U_p(t)dt = 2Af \tag{6}$$

For the operating conditions described in this paper, the U_{pm}/U_0 ratio ranges from to 2 to 13. In pulsed flow, an inversion of the flow occurs at every half period because U_{pm}/U_0 is superior to 1 [27].

In the Nitech-COBR, this ratio to be in plug-flow conditions is located between 2 and 6 [28] (Table 3).

Two dimensionless numbers are defined to characterize the flow:

- the net flow Reynolds number

$$\mathrm{Re}_n = \frac{U_0 D_c}{v} \tag{7}$$

where v is the kinematic viscosity and D_c a characteristic diameter

- the oscillatory Reynolds number to take into account the oscillation conditions

$$\mathrm{Re}_o = \frac{2AfD_c}{v} \tag{8}$$

depending on the mean velocity $U_p = 2Af$.

Table 3
Operating conditions.

Systems	Material	Height of packing	Dispersed phase inlet	Φ (% vol.)	Q_{tot} (L h^{-1})	A (mm)	f (Hz)
Water/PVA/toluene	Stainless steel	3 m	Bottom	25	85–141–226	24–38–56	1.17–1.56
				8	141	24–38–52	1.56
		1 m		25	85–141–226	24–38–52	1.17–1.56
	Without packing	0 m			85–141–226	38–52	1.17–1.56
	PTFE	1 m			85–141–226	24–38–52	1.17–.56
		3 m			85–141–226	24–38–52	1.17–1.56
					300–350–375	0	0
				40	85–141–226	24–38–52	1.17–1.56
			After 1 m	25	85–141	24–38–52	1.56
			After 2 m		85	24–38–52	1.56
Water/SDS/toluene			Bottom		85–141–226	24–38–52	1.17–1.56
				40	85	24–38–52	1.17–1.56
					141	38	1.56

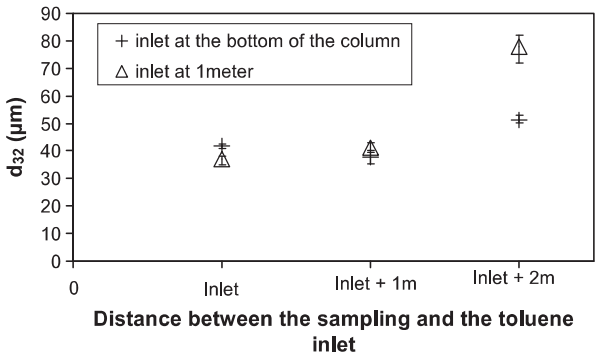

Fig. 5. Sauter mean diameter along the column for different toluene inlet position, water/PVA/toluene system at $\Phi = 25\%$ and 3 m height of PTFE packing, $Q_{tot} = 85$ - L h^{-1}, $A = 52$ mm, $f = 1.56$ Hz.

4.2. Effect of the inlet conditions

The inlet of toluene phase is located at different positions all along the column. Toluene is fed at the bottom of the column ($H = 0$ m) and after 1 of packing ($H = 1$ m). The inserts are made of PTFE.

In Fig. 5, the mean diameter evolution is presented as a function of the corresponding position of the sampling.

If the feeding line is located at the bottom of the column, there are three sample positions: at the inlet ($H = 0$ m), after 1 m ($H = 1$ m), 2 m after the inlet ($H = 2$ m). Obviously, if the inlet is located after 1 m of internal, there are two samplings: at $H = 1$ m (inlet), $H = 2$ m (1 m after the inlet).

The mean droplet sizes obtained are the same at the inlet and at the inlet +1 m for a toluene feed at the bottom or after 1 m of inserts. For an inlet after 2 m of packing, the measurement performed at inlet +1 m corresponds to a sampling at the top of the column and the results do not concur with the other measurements.

4.3. Effect of the operating conditions

For this part, the results refer to the water/PVA/toluene system at a dispersed phase fraction of 25% except if it is specified.

4.3.1. Effect of the oscillation parameters

Fig. 6 shows droplet size distributions for different oscillation velocities, which is defined by the product amplitude by frequency, *Af*, under the same operating conditions (flowrate and holdup) at a sampling position after 1 m of internal.

The striking feature of Fig. 6a is the strong dependence between pulsation velocity and corresponding mean droplet size and droplet size distribution.

Increasing the pulsation velocity leads to smaller droplet size because of the breakage predominance. This result is in agreement with the previous results presented in literature for co-current and counter current designs [19,29,30].

In Fig. 6b, the resulting mean droplet sizes after 1 m of packing are represented versus the *Af* product. The mean droplet size evolution follows a decreasing power law with an exponent of −0.54. Consequently, it is confirmed that the *Af* product plays a major role in the breakup phenomenon.

4.3.2. Effect of the total flowrate

4.3.2.1. Without pulsation. At a flowrate below 300 L h^{-1}, that is to say a net flow Reynolds number lower than 2190, the droplets created are too coarse and no sampling was realized to analyse the droplet size distribution, due to the instability of the dispersion. By increasing the flowrate from 300 ($Re_n = 2190$) to 375 L h^{-1} ($Re_n = 2675$), no influence of the flowrate is noticed (Fig. 7).

All along the first meter, the droplet size is imposed by the droplet generation conditions and the physical properties of the system.

4.3.2.2. With pulsation. In pulsed-flow conditions, no effect of the flowrate is noticed (Fig. 8). The droplet size distributions are perfectly superimposed. The same results are obtained for the whole pulsed conditions investigated. The results are again in accordance with literature results [19,30,34,36]

4.4. Effect of the physical properties

4.4.1. Effect of the surfactant

Even if both involved surfactants lead to the same equilibrium interfacial tension value (Table 1), one has already in mind that the overall adsorption kinetics of these two molecules are different, as well as their nature (PVA: polymeric and non ionic, SDS: molecule anionic).

A simple comparison of this effect due to the nature of the surfactant is given in Fig. 9 for the same operating conditions. The SDS leads to the smallest droplet sizes

Referring to Fig. 3a and b which represent the evolution of the interfacial tension along the column, the PVA interfacial tension is higher than the SDS interfacial tension value in the residence time range. The droplet size difference between the two systems is related to the transient value of the interfacial tension.

Provided that the surfactant concentration is above the critical micellar concentration, the superficial excess concentration and interfacial molecular area are given in Table 4 for both surfactants.

The excess concentration is defined by the Gibbs equation:

$$\Gamma = \frac{1}{RT}\frac{d\sigma}{d\ln c} \tag{9}$$

For polymeric compounds, the Gibbs equation can be applied to polymer with the following formula [35]

$$\Gamma = \frac{\overline{M_{sequence}}}{RT}\frac{d\sigma}{d\ln c} \tag{10}$$

It corresponds to the concentration of surfactant at the interface when it has just been covered by the molecules. This concentration is superior when using PVA.

A, area occupied by a surfactant molecule at the liquid–liquid interface, can be deduced from this excess concentration Γ. A PVA molecule requires a larger space than a SDS molecule.

Consequently, less PVA molecules are required to stabilize the interface. However, because of the sterical cluttering, the droplet sizes obtained are larger with PVA than with SDS. Due to the larger size of the PVA molecule, the surfactant adsorption is followed by a rearrangement of the molecule at the interface.

It explains why larger droplet size is obtained with the PVA surfactant.

4.4.2. Effect of the dispersed phase holdup

The dispersed phase holdup can affect the mean droplet size. It is a relevant parameter in the batch process.

Fig. 10a shows a difference in the droplet size distribution between low dispersed phase (8%) and higher dispersed phase holdups (25% and 40%). At 8% in volume, a lower coalescence probability may be expected. At higher dispersed phase holdups, the interdroplet coalescence may occur despite the presence of surfactant, and consequently, the droplet size distributions are shifted to the right, i.e. to larger droplets. However no relevant difference is noticed between 25% and 40% of volumetric dispersed phase fraction.

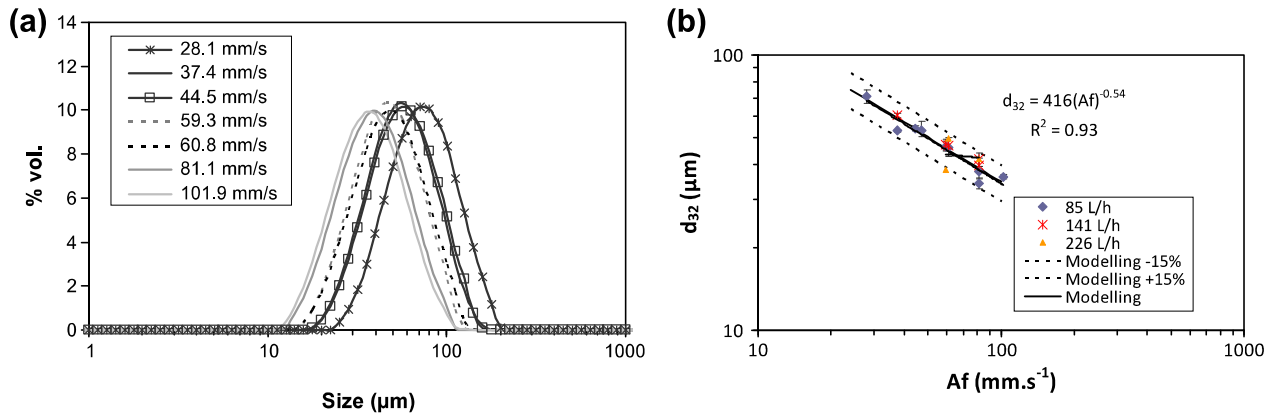

Fig. 6. (a) Droplet size distributions evolution with the *Af* product (system water/PVA/toluene, Q_{tot} = 85 L h^{-1}, Φ = 0.25, H = 1 m, bottom introduction, 3 m of PTFE packing) (b) evolution of the mean droplet diameter with the *Af* product (system water/PVA/toluene, Φ = 0.25, H = 1 m, bottom introduction, 3 m of PTFE packing).

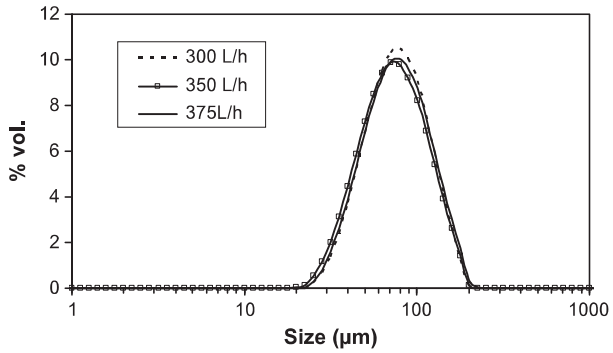

Fig. 7. Droplet size distributions evolution with the total flowrate Q_{tot} (system water/PVA/toluene, without pulsation, Φ = 0.25, H = 1 m, bottom introduction, 3 m of PTFE packing).

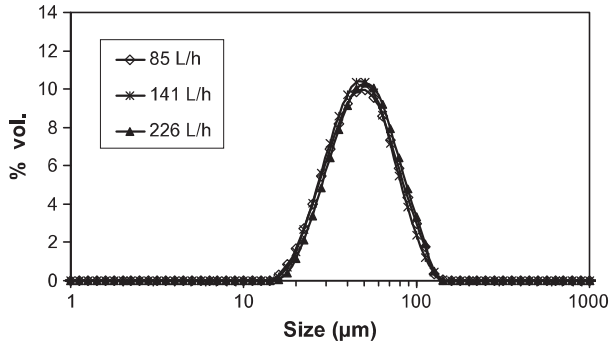

Fig. 8. Droplet size distributions evolution with the total flowrate Q_{tot} under the same pulsation conditions (system water/PVA/toluene, A = 52 mm, f = 1.17 Hz, Φ = 0.25, H = 1 m, bottom introduction, 3 m of PTFE packing).

Fig. 10b presents the Sauter mean droplet size at a given flowrate for three stainless steel meters of internal and different pulsation conditions with the water/PVA/toluene system. For a dispersed phase fraction of 8%, the Sauter mean diameter is slightly inferior to the diameters obtained with the two other hold-ups. No significant difference is noticed between the two higher dispersed phase holdups.

In conclusion, no major influence on the drop size distribution at high volume dispersed phase holdup (superior than 25% up to 40%) is expected, provided that it results from an equilibrium between breakage and coalescence. On the contrary, the size distribution seems to be sensitive to coalescence when the dispersed phase holdup ranging from some percent to 25% in volume.

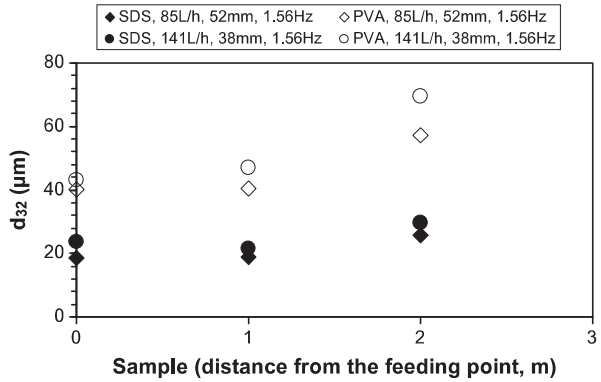

Fig. 9. Mean droplet size under different condition for the both systems (Φ = 0.25, bottom introduction, 3 m of PTFE packing).

Table 4
Calculation of the excess concentration Γ and of the interfacial molecular area A for both systems.

	System SDS	System PVA
Excess concentration Γ mg m^{-2}	0.59	0.87
Interfacial molecular area A Å^2 molecule^{-1}	80.9	3499

4.5. Effect of the inserts

These results are reported with the Water/PVA/Toluene system.

Two parameters have been considered: the presence of inserts and the internal length and the nature of the inserts materials (stainless steel or PTFE). Both effects depend on the disc and doughnut materials.

4.5.1. Effect of the height of the internal

The effect of the height of the internal on the mean droplet size and on the droplet size distribution is inquired through three different configurations. The results are presented without internal, with internal only on the first meter of the column and with internal all along the column. For the last two cases, it is interesting to compare the results obtained with both internal materials:

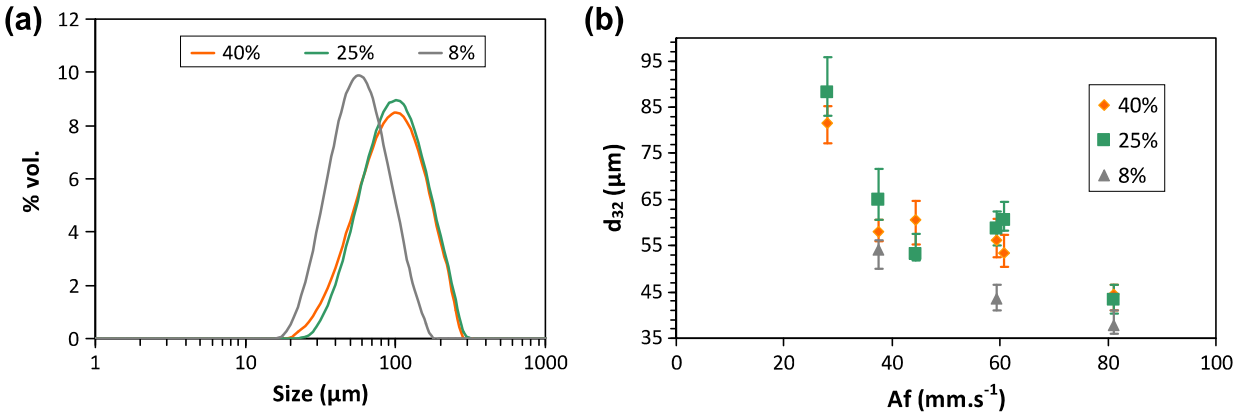

Fig. 10. a) Droplet size distribution for the three dispersed phase concentration (bottom introduction, 3 m of stainless steel packing, Q_{tot} = 141 L h^{-1}, A = 24 mm, f = 1.56 Hz, sampling after on meter of packing H = 1 m) (b) Sauter mean droplet size versus the Af product for the three dispersed phase concentration (bottom introduction, 3 m of stainless steel packing, Q_{tot} = 141 L h^{-1}, H = 1 m).

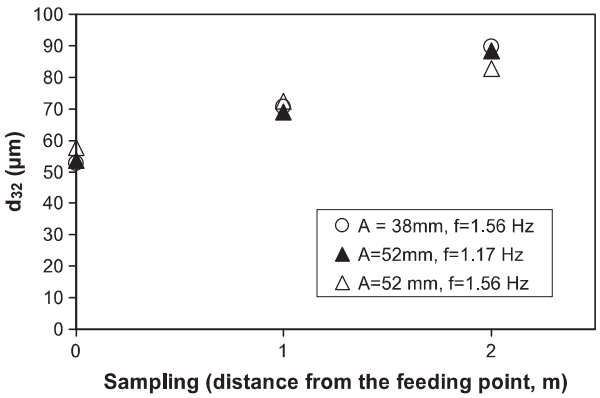

Fig. 11. Mean Sauter diameter along the column for different pulsation condition at Φ = 0.25, Q_{tot} = 85 L h^{-1} bottom introduction, without packing.

stainless steel and PTFE which both present different wettability characteristics (Table 2).

4.5.1.1. Without insert. Fig. 11 presents mean droplet size variation along the column without internal.

The oscillation conditions have no effect on the Sauter mean droplet size. It is only controlled by the properties of the systems and by the inlet phase conditions. The Sauter mean droplet size increases along the column from 55 µm to 90 µm.

4.5.1.2. With PTFE or Stainless steel inserts. Figs. 12 and 13 present the respective evolutions of the Sauter mean droplet size and droplet size distributions with stainless steel inserts respectively for 1 m and for 3 m of inserts in the column. Figs. 12a and 13a present the mean droplet sizes all along the column according to different pulsation conditions. Figs. 12b and 13b correspond to DSD obtained at the first meter sampling.

With inserts all along the column (Fig. 12a–b), the pulsation is the main parameter which affects the drop breakage.

However, with just 1 m of inserts (Fig. 13a–b), the oscillation conditions do not affect the droplet size. All the mean droplet size and droplet size distributions are superimposed which suggests a breakage controlled by the inlet conditions and the physical properties of both systems.

Concerning PTFE inserts, both heights of inserts and operating conditions control the mean droplet size (Fig. 14). Indeed, an increase of the pulsation velocity as well as an increase of the inserts height contributes to a decreasing mean droplet size (Figs. 14a–b and 15). The PTFE is known to be an inert material whereas stainless steel properties may change in time (from hydrophilic to hydrophobic). Consequently, in the case of a PTFE insert, the operating conditions are expected to control the mean droplet size, much more than in the case of stainless steel.

4.5.2. Effect of the insert materials

In Fig. 16, two operating conditions are reported with 3 m of internal under two different operating conditions.

The same trends mentioned above are observed: there is an increase of the mean droplet size all along the column and an increase of the amplitude leads to smaller droplet sizes.

The smallest droplet sizes are obtained with PTFE internals.

5. Modeling of the experimental results

5.1. Prediction of the mean droplet size existing correlations

Lots of correlations are available in literature to predict the mean droplet size in pulsed columns. Most of them deal with counter-current flow. Some others correspond to the co-current continuous oscillatory baffle reactor (Nitech).

Some of the most important correlations are listed in Table 5. Different dimensionless numbers are committed depending on the pulsation (Af), the physical properties (interfacial tension, viscosity and density) and the internal geometry (T, transparency factor).

Other papers are available in literature which are based on population balance equation, able to predict the drop size distribution, provided that break-up and coalescence models are implemented [1]. The originality of the work proposed in the following section concerns liquid–liquid dispersion study in discs and doughnuts pulsed column in a co-current upflow. The literature is relatively extended concerning oscillatory baffled reactor (OBR) even if it is often limited to batch or liquid–liquid systems without surfactant, whereas for discs and doughnuts pulsed column, few studies concern upward co-current flow.

5.2. Modeling of the mean droplet size with the energy dissipation rate

5.2.1. Literature

Jealous and Johnson [37] first evaluated the power dissipation in pulsed column using a quasi steady state model. The model assumed that the flow is fully developed at any moment within the

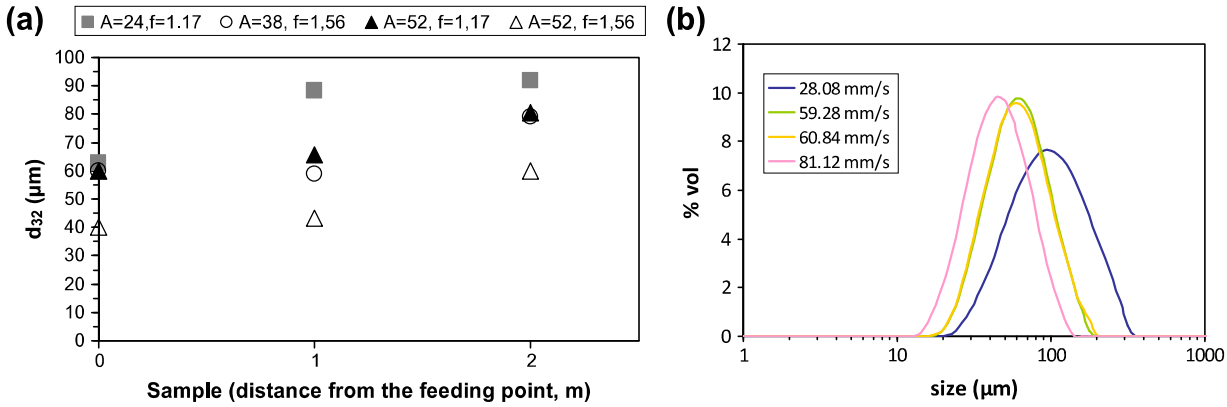

Fig. 12. (a) Mean Sauter diameter along the column for different pulsation condition at $\Phi = 0.25$, $Q_{tot} = 85$ L h^{-1} bottom introduction, 3 m of stainless steel packing and (b) droplet size distribution for the corresponding *Af* product at $H = 1$.

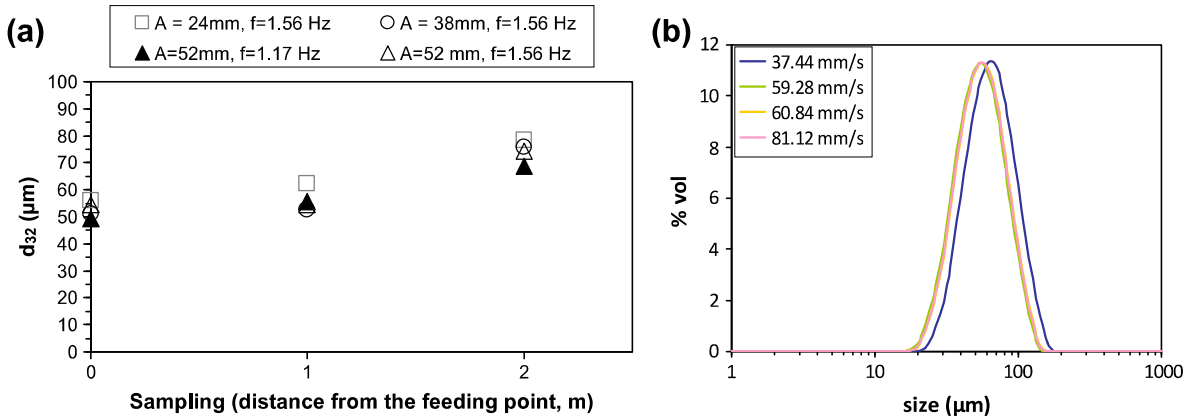

Fig. 13. (a) Mean Sauter diameter along the column for different pulsation condition at $\Phi = 0.25$, $Q_{tot} = 85$ L h^{-1} bottom introduction, 1 m of stainless steel packing and (b) droplet size distribution for the corresponding *Af* product at $H = 1$.

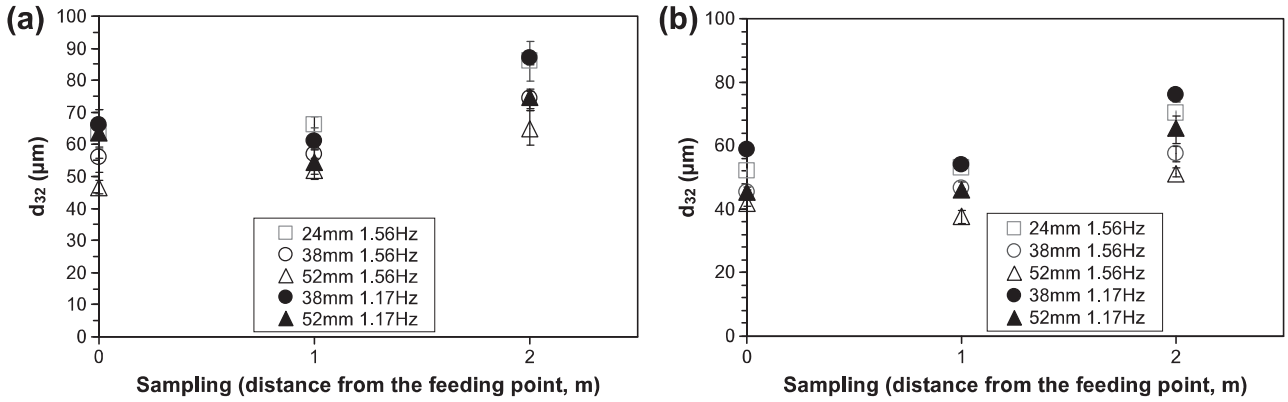

Fig. 14. Mean Sauter diameter along the column for different pulsation condition at $\Phi = 0.25$, $Q_{tot} = 85$ L h^{-1} bottom introduction, with PTFE packing on (a) 1 m height and (b) on three meter height.

fluid oscillation. These authors related the instantaneous power consumption to the static pressure, to the inertia force to accelerate the liquid and to the hydrodynamic frictional force imposed by the baffle and other fittings. The power dissipation rate ε is expressed as:

$$\varepsilon = \frac{P}{\rho V} = \frac{16\pi^2 N}{3C_d^2}\frac{(1-T^2)}{T^2}(x_0 f)^3 \quad (\mathrm{W\ kg^{-1}}) \tag{11}$$

where N is the number of baffled cells per unit length (m^{-1}), T fractional free area defined as $\left(\frac{D_0}{D}\right)^2$ where D_0 and D are the orifice and tube diameter (m) respectively and C_d the orifice coefficient for the flow through the baffle hole and is assumed to be 0.6 for fully developed conditions. f is the oscillation frequency and x_0 is the oscillation amplitude center-to-peak corresponding to $A/2$. Baird and Stonestreet [38] noticed that the previous law fits well at large amplitudes A and low frequency f.

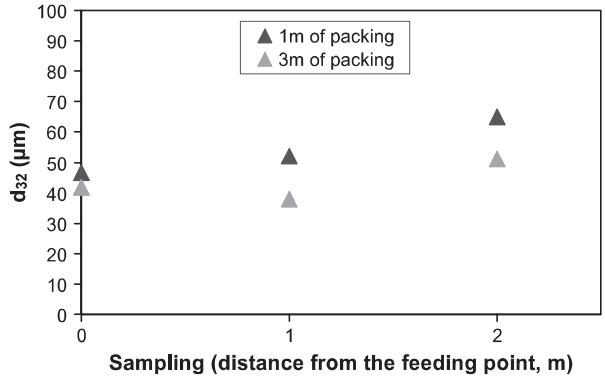

Fig. 15. Mean Sauter diameter along the column for two different height of PTFE packing $\Phi = 25\%$, $Q_{tot} = 85\ L\ h^{-1}$, $A = 52$ mm, $f = 1.56$ Hz bottom introduction.

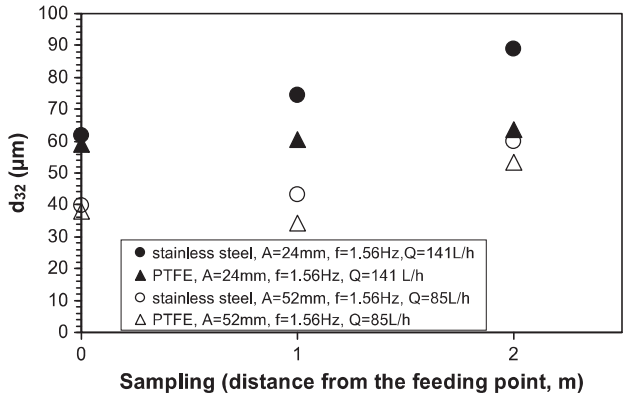

Fig. 16. Effect of the packing on the mean Sauter diameter along the column.

For the lower amplitudes (5 mm) and higher frequencies (3–14 Hz), they proposed a new flow model based on acoustic principles and eddy viscosity:

$$\varepsilon = 1.5\frac{(2\pi f)^3 x_o^2 l}{HT} \quad (\mathrm{W\ kg^{-1}}) \tag{12}$$

l is the mixing length (m) which is an adjustable parameter of the same order of the pipe diameter and H the baffle spacing (m).

In his PhD, Aoun Nabli [39] establishes a correlation of the mean energy dissipation for oscillating flow in disc and doughnut columns (no net flowrate in the column). The velocity is defined like in the expression (5).

$$\frac{\langle\varepsilon\rangle D}{(2Af)^3} = 1.4\times 10^3\left(\frac{1}{h^*}\right)^{1.29}\left(\frac{1}{T^*}\right)^{1.34}\left(\frac{1}{A^*}\right)^{0.37}(f^*)^{0.62} \tag{13}$$

for $h^* = 0.156$–0.406, $T^* = 17$–40%; $A^* = 0.057$–0.200; $f^* = 55{,}406$–$124{,}582$.

The different ratios, characterizing the inserts shape ratio (15), the frequency (16) and the amplitude parameters (17) are defined below:

$$h^* = \frac{H}{D} \tag{14}$$

$$f^* = \frac{fD^2}{\nu} \tag{15}$$

$$A^* = \frac{A}{D} \tag{16}$$

5.2.2. Modeling of the mean Sauter diameter with the mean energy dissipation rate

The correlation of Jealous and Johnson [37] has been used to calculate the mean energy dissipation rate (11).

The d_{32} and d_{90} are related with a classical proportional relationship ($d_{90}/d_{32} = 1.9$). So the mean Sauter diameter evolution can be represented versus the mean energy dissipation rate [40].

Fig. 17 represents the mean Sauter diameter-energy dissipation rate plot for the two studied systems and for both inserts. The mean droplet size corresponds to the size obtained after 1 m of inserts.

Table 5
Mean droplet size expression in different pulsed column.

References	System	Flow	Correlations
[32,33]		Counter current pulsed sieve plate column	$\frac{d_{32}}{\sqrt{\sigma/\Delta\rho g}} = 1.35\varepsilon^{0.4}\left(\frac{h_c\sqrt{\rho_* g}}{\sigma_*}\right)^{0.18}\left(\frac{\mu_d g^{1/4}}{\rho_*^{1/4}\sigma_*^{3/4}}\right)^{0.14}\left(\frac{\sigma}{\sigma_*}\right)^{0.06}\times\left[0.23+\exp\left(-26.66\frac{Af^2}{gc}\right)\right]$ $\varepsilon = \frac{2\pi^2(1-T^2)}{3T^2C_0^2h_c}(Af)^3$ $\frac{d_{32}}{H} = \frac{C_\psi e^n}{\frac{1}{C_\Omega\left(\frac{\sigma}{\Delta\rho g H^2}\right)^{0.5}}+\frac{1}{C_\Pi\left[\left(\frac{\psi}{g}\right)\left(\frac{\Delta\rho}{g\sigma}\right)^{0.25}\right]^{n_1}\left[H\left(\frac{\Delta\rho g}{\sigma}\right)^{0.5}\right]^{n_2}}}$
[33]		Counter current disc and doughnut pulsed column	$\frac{d_{32}}{\sqrt{\sigma/\Delta\rho g}} = C_1 e^{n_1}\left(h_c\frac{\sqrt{\rho_* g}}{\sigma_*}\right)^{n_2}\left(\frac{\mu_d g^{1/4}}{\rho_*^{1/4}\sigma_*^{3/4}}\right)^{n_3}\left(\frac{\sigma}{\sigma_*}\right)^{n_4}\times\left[C_2+\exp\left(C_3\frac{Af}{e(\sigma_* g/\rho_*)^{1/4}}\right)\right]$ C_1, C_2, C_3, n_1, n_2, n_3 and n_4 are respectively 2.84, 0.16, −2.59, 0.30, 0.18, 0.14, 0.06 ρ_* and σ_*7: density and surface tension of water at 20 °C
[29]	Without mass transfer	Counter currentisc and doughnut pulsed column	$\frac{d_{32}}{\sqrt{\sigma/\Delta\rho g}} = 33.53\times 10^{-3}\left(\frac{Af^4}{g\sigma}\right)^{-0.283}\left(\frac{d_a\rho_c\sigma}{\mu_c^2}\right)^{0.29}\left(\frac{\rho_c\sigma^4}{\psi\mu_c}\right)^{-0.13}\left(\frac{\Delta\rho}{\rho_c}\right)^{2.86}\left(\frac{\mu_d}{\mu_c}\right)^{0.085}\left(\frac{h_c}{d_a}\right)^{-0.734}(1+R)^{0.34}$ $\psi = \frac{2\pi^2(1-T^2)}{3T^2C_0^2h_c}(Af)^3$ H_c: compartment height; e: fractional free area; C_0 orifice coefficient; D_a doughnut aperture diameter; R: flow ratio
[19]	Without surfactant	Co current continuous oscillatory baffled reactor	$d_{32} = 1.72\times 10^{-2}\mathrm{Re}_0^{-0.91}\mathrm{Re}_n^{-0.42}$ (m) $d_{32} = 3.7\times 10^{-5}\varepsilon^{-0.3}\varepsilon_n^{-0.14}$, $3.18 \le \varepsilon \le 25\ \mathrm{W\ kg^{-1}}$ ε energy dissipation due to power input; ε_n energy dissipation due to the net flow
[31]	Without surfactant	Co current continuous oscillatory baffled reactor	Vertical COBR – Riser $\frac{d_{32}}{D} = 0.40(\pm 54\%)\mathrm{Re}_0^{-0.57(\pm 17.72\%)}\mathrm{Re}_n^{0.31(\pm 12.25\%)}$ ($R_2 = 0.744$) – downcomer: $\frac{d_{32}}{D} = 1.24(\pm 41.88\%)\mathrm{Re}_0^{-0.66(\pm 10.9\%)}\mathrm{Re}_n^{0.29(\pm 15.65\%)}$ ($R_2 = 0.867$) Horizontal COBR $\frac{d_{32}}{D} = 107\mathrm{Re}_0^{-0.90}\mathrm{Re}_n^{0.13}$

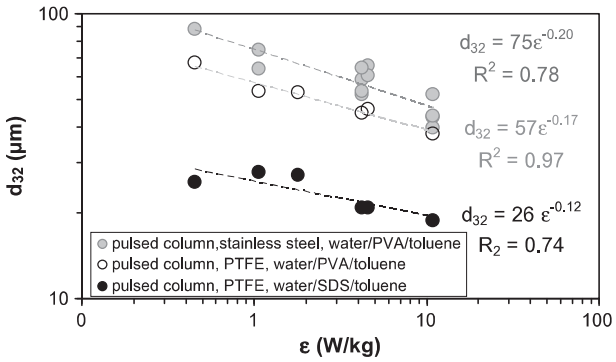

Fig. 17. Mean droplet size versus the energy dissipation for the three systems combination at $\Phi = 25\%$, $h = 1$ m.

Theoretically, the Kolmogorov cascade theory assumes a decreasing power law versus the energy dissipation rate with an exponent equal to −0.40 under the assumption of isotropic homogeneous turbulence [41]. In the studied operating conditions, the decreasing is less important, the fitting exponents ranging from −0.12 to −0.20. For the break-up mechanism, it exhibits a weaker dependency on the turbulent flow patterns than on the interactions with the inserts. Obviously, the operating parameters are strongly involved in the breakage and coalescence balance as mentioned previously (Section 4.3) but this effect is dampened compared to the inserts influence caused especially by the wettability property.

In previous works, various values of exponents can be found. For instance, in the work of Gourdon [42], the pulsed column and the rotary-agitated Kühni column have been compared. The maximum stable diameter follows a decreasing power law according to the energy dissipation rate with an exponent of −0.25 for the pulsed column and −0.55 for the Kühni column. In the Pereira work [19], the exponent values are really close to ours, with an exponent of −0.16 for a vertical COBR in the riser and of −0.23 in the downcomer.

Most of the time, these different exponent values account for the actual flow conditions that are not perfectly homogeneous and isotropic as in theory.

Since the dispersed phase fractions investigated in our work are higher than the classically ones found in literature, we have tried in the next section to apply the up-to-date breakage and coalescence models to our conditions in order to explain the evolution of our experimental characteristic drop diameters. The aim is just here to detect the respective roles of breakage and coalescence.

5.3. Breakage and coalescence frequencies

This section focuses on the understanding of the breakage and coalescence phenomena which occur during the pulsating flow. The different models of coalescence and breakage of the literature are presented. Then, coalescence and breakage frequencies are roughly estimated. Our goal is not to propose a new model related to our process and to our phase system, but just to estimate them in order to point out which mechanism should be predominant in our liquid–liquid dispersion system.

There are lots of models available in the literature. The first two parts are devoted to a short explanation of the models chosen in this work. Finally, the respective breakage and coalescence frequencies are evaluated by using our experimental conditions (physical properties, energy dissipation, etc.).

5.3.1. Coalescence frequency

Lots of correlations are described in literature to estimate the coalescence frequency. The calculations of the coalescence frequency are based on the works of Chesters [44] and the review of Lia and Lucas [43].

The interdrop coalescence frequency is represented as the product of the coalescence efficiency, P, with the collision frequency, C, the latter being defined by the following expression:

$$C = k v d^2 n^2 \tag{17}$$

where d represents the characteristic droplet diameter and n the number of droplets by volume unit. This expression is directly derived from the collision theory of Smoluchosvski. The k constant and the relative collision velocity, v, depend on the hydrodynamics conditions which lead to the interdrop collision. These conditions are defined thanks to the comparison of the drop size with some of the characteristic flow scales. Generally, in turbulent flows, there is an usual scale, which represents the limit between the inertial domain and the viscous one. This is the Kolmogorov length scale, calculated via the following relationship:

$$\lambda_K = \left(\frac{\nu^3}{\varepsilon_m}\right)^{1/4} \tag{18}$$

where ν is the kinematic viscosity and ε_m is the mean energy dissipation rate (W kg^{-1}). It is the scale representative of viscous dissipation (Kolmogorov energy cascade).

Comparing droplet size, d, with the Kolmogorov length scale, it is possible to define whether the interdrop collision occurs in the viscous domain or in the turbulent inertial sub range. The respective parameters k and v for the collision rate are classically expressed according to the drop size d versus λ_K (Table 6).

In Fig. 18, the comparison of our experimental Sauter diameter with the Kolmogorov scale is plotted as a function of the mean energy dissipation rate.

As it can be seen, the mean Sauter diameter and the Kolmogorov length scale are in the same range, but, within the whole range of dissipation rates, the experimental d_{32} remain larger than the Kolmogorov length scale. It implicitly means that the collisions happen to be governed by the turbulent inertial regime.

For the coalescence efficiency P, different models are available in the literature. Generally, it is linked to two characteristic times, the film drainage time and the interdrop collision time (contact time), as follows:

$$P = \exp\left(-\frac{t_{drainage}}{t_{contact}}\right) \tag{19}$$

The contact time can be estimated by:

$$t_c \approx \frac{d_{32}}{v} \tag{20}$$

v being the relative collision velocity.

The drainage time is much more difficult to be predicted. We refer here to the work of Chesters [44], who proposed the following expression:

$$t_{drainage} = t_{ch} \ln\left(\frac{h_c}{h_0}\right) \tag{21}$$

where t_{ch} is a characteristic time defined such as:

$$t_{ch} = \frac{3\pi\mu_c R^2}{2F} \tag{22}$$

Table 6
Parameters k and v for the collision rate.

	v	k
Inertial subrange: $d > \lambda_K$	$v = (\varepsilon d)^{1/3}$	$\left(\frac{8\pi}{3}\right)^{1/2}$
Viscous turbulent flow: $d < \lambda_K$	$v = (\varepsilon\nu)^{1/2} d$	$\left(\frac{2\pi}{15}\right)^{1/2}$

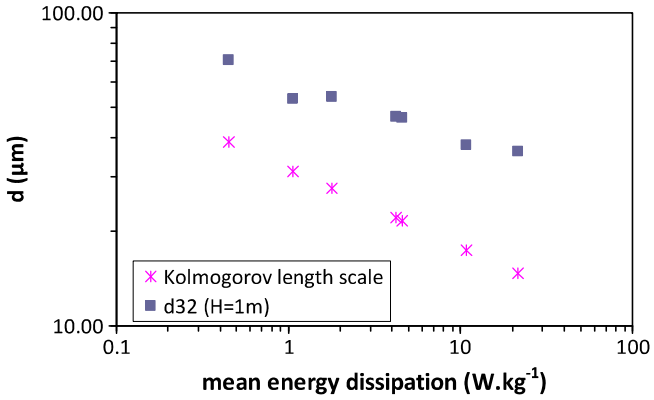

Fig. 18. The mean droplet size and the Kolmogorov length scale versus mean energy dissipation.

with F an interaction force (R being the drop radius):

$$F = 6\pi\mu_c R^2 \sqrt{\frac{\varepsilon_m}{\nu_c}} \tag{23}$$

and h_c the critical film thickness corresponding to the continuous film rupture and expressed by:

$$h_c = \left(\frac{AR}{8\pi\sigma}\right)^{1/3} \tag{24}$$

where A is the Hamaker constant, generally taken equal to 10^{-20} J.

In Fig. 19, the coalescence frequency can be evaluated versus the drop diameter for a given energy dissipation rate. It is expected that the coalescence frequency is decreasing with the mean droplet size.

5.3.2. Breakage frequency

Recently, a broad and detailed overview of the existing laws was given in the papers of Liao and Lucas [45] and in the work of Maass and Kraume [46].

For instance, the well-known mechanistic model for the drop breakage rate proposed by Coulaloglou and Tavlarides [47] assumes that the breakage frequency is the product of the fraction of the total number of breaking drops and the reciprocal time needed for the drop breakage to occur. The breakage frequency is then defined by expression (25).

$$k_{Br} = B_1 \frac{\varepsilon^{1/3}}{d^{2/3}} \exp\left(B_2 \frac{\sigma}{\rho_C \varepsilon^{2/3} d^{5/3}}\right) \tag{25}$$

B_1, B_2 are fitting constants. Traditionally, each author presents his own set of parameter values based on trial-and-error attempts to reproduce experimental results in liquid–liquid application.

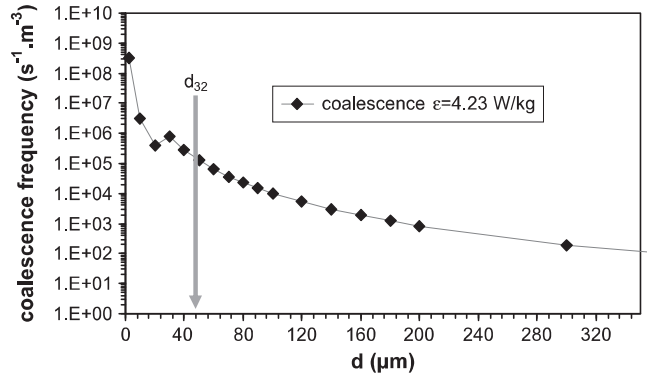

Fig. 19. Coalescence frequency evolution versus drop diameter for a given energy dissipation rate.

Maass and Kraume [46] and Ribeiro et al. [48] present tables of values from literature [45–48]. Depending on the authors and the conditions and studied systems, B_1 ranges from 6.16×10^{-4} [48] to 9.1×10^{-1} [46]. In the same way, B_2 varies from 5.7×10^{-2} [50] to 4.1 [47]. It appears that the different fitting parameters whatever the model are varying according to several orders of magnitude.

To take into account the dispersed phase fraction Φ, the initial Coulaloglou and Tavlarides model (26) is corrected as follows:

$$k_{Br} = B_1 \frac{\varepsilon^{1/3}}{(1+\phi)d^{2/3}} \exp\left(B_2 \frac{\sigma(1+\phi)^2}{\rho_c \varepsilon^{2/3} d^{5/3}}\right) \tag{26}$$

It allows to account with the damping effect on the turbulence level induced by the dispersed phase fraction.

Determining the breakage constants couple (B_1, B_2) is then a major challenge.

In our case, so as to get the order of magnitude of these (B_1, B_2) parameters it is assumed that the maximum stable diameter may be roughly assimilated to the d_{90} experimentally found, since above this size limit the drops are expected to break-up and to disappear. Consequently, it is assumed that the breakage probability may be considered as quasi null (10^{-5}) at this drop size value.

First, the different values of B_1 taken from the literature [46–49] have been implemented and by this way, the corresponding B_2 values have been identified (Table 7). With significant B_1 variation (10^{-4} to unity) no major evolution of B_2 is noticed. These values are in the same range as the ones usually found in literature.

So B_2 is arbitrarily fixed to an averaged value of 0.79. B_1 is calculated with the same method. B_1 varies by several orders of magnitudes (Table 8).

But B_1 has a physical meaning, provided that it has to be considered as a proportional coefficient between the contact and the breakage times (28), such as:

$$t_{Br} = \frac{t_C}{B_1} \tag{27}$$

where t_c is the contact time expressed by (20) which is equivalent to the eddy life time.

To get a successful breakage, it is important to emphasize that the breakage time has to be lower than the life time of an eddy. Consequently, in our opinion, B_1 must be larger than one and the values identified as being inferior to 1 in Table 8 can be forgotten. Finally, it seems that in the literature the breakage time values are close to our contact times. In conclusion, the B_1 constant has been estimated in this work by assuming that the breakage time is at least 1.5 times lower than the contact time. It leads to our proposal to set a B_1 constant equal to 1.5.

5.3.3. Application to the pulsed column case

These models allow the understanding of the phenomena that happened in the different compartments of our discs and doughnuts column.

At a given investigated operating condition, three characteristic drop diameters are described (Fig. 20):

Table 7
Values of B_2 for a zero breakage frequency for the different literature B_1 value under our experimental energy dissipation rate.

ε (W kg^{-1})	B_1	B_2
[0.45;21]	0.91	[0.42;1.8]
	0.86	[0.42;1.8]
	6.14×10^{-4}	[0.25;1.09]
	0.336	[0.36;1.7]

Table 8
B_1 values at a given B_2 and the corresponding characteristic times in the range of our experimental dissipation rate.

B_2	B_1
0.79	$[2.65 \times 10^{-5}; 7.74 \times 10^{7}]$

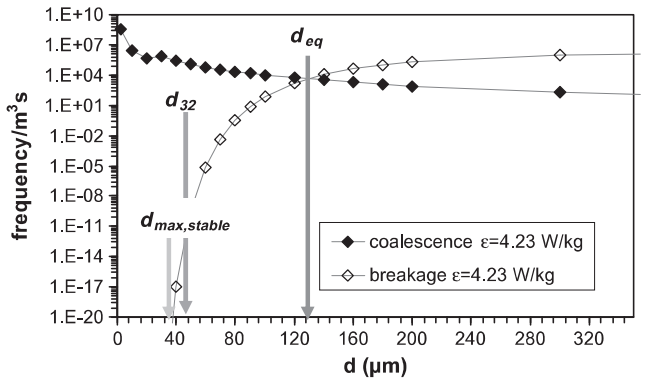

Fig. 20. Breakage and coalescence frequencies evolution with droplet diameter and identification of three characteristics diameter of the dispersion.

- The experimental mean Sauter diameter d_{32} measured with the Malvern Mastersizer 2000 analysis ($H = 1$ m).
- The maximum stable diameter $d_{\max,\text{stable}}$ which is evaluated thanks to the breakage frequency theory and corresponds to the maximum stable droplet size. It corresponds to the drop diameter for which the breakage frequency is equal to zero. Experimentally, a first approximation would have it assimilated to d_{90}.
- The equilibrium diameter d_{eq} defined as the diameter for which the coalescence and breakage frequencies are equal.

The calculation of the frequencies assumes that coalescence occurs between equal sized droplets alone.

At a diameter lower than d_{eq}, the coalescence frequency is superior to the breakage frequency. Consequently, coalescence becomes predominant in its balance with breakage. On the contrary, for a diameter superior to d_{eq}, the breakage frequency is superior to the coalescence frequency. In this case, breakage prevails.

To summarize all the results, Fig. 21 represents the evolution of these three characteristic diameters versus the turbulent energy dissipation rate.

First of all, in our case the equilibrium diameter d_{eq} is always superior to the maximum stable diameter and consequently to d_{32}. Therefore, in the balance between breakage and coalescence, coalescence is expected to be the prevailing mechanism which affects the droplet size and the droplet size distribution.

Considering the different dispersed phase holdups (Fig. 21), the breakage frequency is modified and consequently, the maximum stable diameter and the equilibrium diameter too.

With an increase in the dispersed phase holdup, the d_{eq} and the $d_{\max,\text{stable}}$ are larger than those calculated at lower dispersed phase holdup. However, the mean Sauter diameter is not affected by the dispersed phase holdup (Section 4.4.2).

5.4. Modeling of the mean droplet size evolution through dimensionless numbers

As presented in Table 5, the mean diameter evolution can be presented via dimensionless numbers. Accounting with the dependency of droplet size pointed out previously, the evolution is presented through the oscillatory Reynolds number (Eq. (8)) to take into account the oscillation effect on droplet size (Fig. 22).

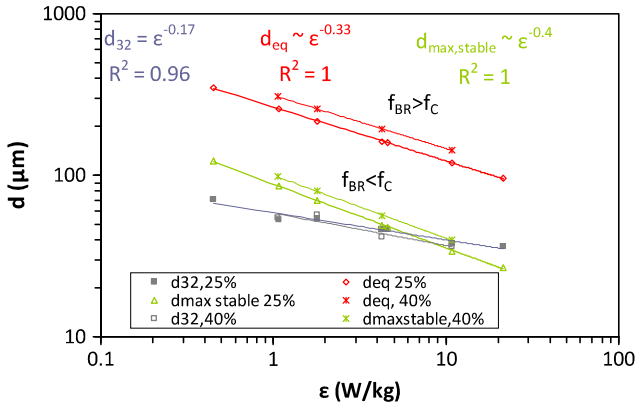

Fig. 21. The three characteristics diameter variations with the mean energy dissipation rate for the water/PVA/toluene system by taking into account the dispersed phase concentration in the calculation of the frequencies.

The evolution presents a power law in the same range, whatever the inserts material. The only difference can be explained by the surface wettability. So it has to be taken into account in the correlation.

In the case of the PTFE inserts, the difference between the Sauter diameter evolutions can be explained thanks to the interfacial tension. Consequently the dimensionless Weber number is also a relevant dimensionless number.

To take into account the adhesion work (expression 29) in which intervenes the interfacial tension and the contact angle, a special Weber number is defined. It corresponds to the ratio between the inertial energy and the interfacial energy. This specific dimensionless Weber We_s is expressed as follows:

$$We_s = \frac{E_{inertial}}{E_{adhesion}} = \frac{\rho_c U^2 d_h^3}{\sigma(1+\cos\theta)d_h^2} = \frac{\rho_c U^2 d_h}{\sigma(1+\cos\theta)} \tag{28}$$

$$W_{ad} = \sigma(1+\cos\theta) \tag{29}$$

U is the velocity related to the fluid displacement. The fluid displacement is due to the pulsation and to the net flow. Consequently, the specific dimensionless Weber number We_s is expressed by:

$$We_s = \frac{\rho_c (U_0 + 2Af)^2 d_h}{\sigma(1+\cos\theta)} \tag{30}$$

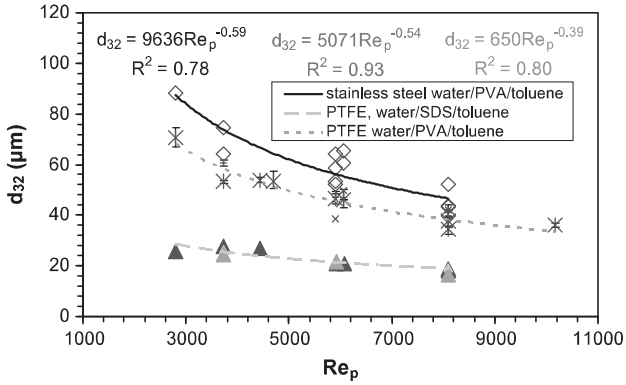

Fig. 22. Mean Sauter diameter versus the pulsation Reynolds number for the three systems at $\Phi = 25\%$ and $H = 1$ m.

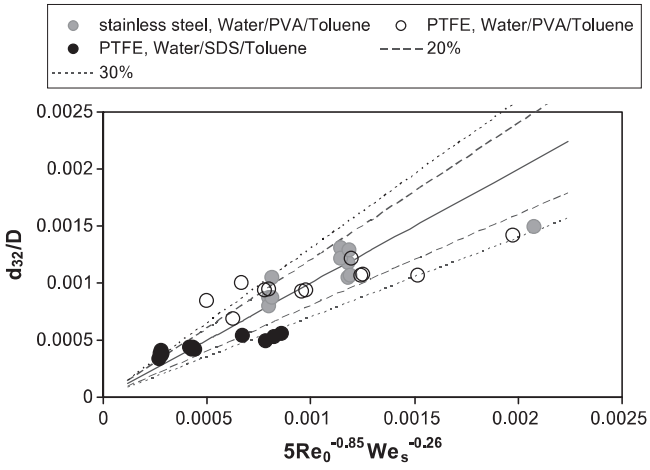

Fig. 23. Comparison between the model and the experimental results.

where U_0 is the net flow velocity and $2Af$ the mean pulsation velocity.

The dimensionless Weber number is calculated by taking the interfacial tension value at a time corresponding to the residence time after one meter of insert in the column.

A dimensionless correlation aiming towards the prediction of the Sauter diameter relatively to the column diameter, by taking into account the oscillatory flow Reynolds number Re_o and the specific Weber number We_s is expressed as

$$\frac{d_{32}}{D} = C\mathrm{Re}_o^{\alpha} We^{\beta} \tag{31}$$

The different coefficients C, α and β are evaluated by using the mean square method for each set of experiments by the mean square method. Then an average of the coefficients provides the value for the correlation.

The fitting correlation is finally expressed as:

$$\frac{d_{32}}{D} = 5\mathrm{Re}_o^{-0.85} We_s^{-0.26} \tag{32}$$

Fig. 23 allows the comparison between experimental and model data.

This error range is reasonable given that the measurement uncertainty on the mean droplet size (sampling, measurement method), contact angle, flowrate, oscillation, etc. This representation fits our data but do not claim to be a general correlation which then requires additional runs.

6. Conclusion

The disc and doughnut pulsed column is used here co-currently to create a liquid–liquid dispersion. Despite the use of a surfactant, it seems that a coalescence phenomenon occurs in the last meter of the column. Different parameters have been investigated and their effect on the mean droplet size has been studied.

Concerning the operating parameters, it is suggested that the net flow rate has no significant effect. Moreover, the most important operating parameter is the pulsation velocity characterized by its oscillation amplitude and frequency product. An increase in pulsation velocity leads to a smaller mean droplet size. Besides, in the same pulsation conditions, the residence time can be modified without effect on the dispersion properties. According to the application, the residence time can then be controlled.

Concerning the physical properties, the nature of the surfactant has been investigated. Both surfactants (PVA and SDS) lead to the same value of interfacial tension at equilibrium. However, their nature and adsorption mechanism are different. Larger mean droplet sizes are obtained with PVA which is characterized by larger molecules than SDS.

The dispersed phase holdup has also been studied. At a high concentration (25% and 40%) no effect is pointed out. However, with more diluted liquid–liquid dispersion, the mean droplet sizes obtained are smaller. So, at higher dispersed phase holdup, the coalescence and breakage frequencies balances are modified.

Concerning the inserts, their nature affects both the mean droplet size and the behavior of the dispersion according to the height of inserts. Without inserts, the mean droplet size is not influenced by the hydrodynamics because whatever the operating conditions, the same drop sizes are obtained. It means that the mean droplet size is only governed by the initial conditions. In case of PTFE inserts, the hydrodynamics controls the mean droplet size: the droplet size distribution and the mean droplet sizes evolve with the pulsation velocity and the height of the inserts. On the contrary, with stainless steel inserts, with just 1 m of inserts, the mean droplet sizes do not evolve with the pulsation conditions. The liquid–liquid dispersion is then influenced by the nature and height of the inserts. The comparison between both types of inserts has been performed under the same other operating conditions. It appears that smaller mean droplet sizes are obtained with PTFE inserts than with stainless steel inserts. This result is unexpected given that the PTFE is preferentially wetted by the dispersed phase. Maybe smaller droplets are detached from the discs or doughnuts and modify the droplet size distribution obtained.

The evolution of the mean Sauter diameter is modeled through different correlations. Regarding the results obtained in terms of mean energy dissipation rate, it seems that the turbulence is mainly affected by the inserts geometry.

A dimensionless correlation to predict the mean droplet size is proposed. It takes into account the interfacial tension of the system as well as the inserts nature. In addition to the classical dimensionless numbers characterizing the pulsed flow (Re_n and Re_p), the Weber number We_S depending on the interfacial tension and on the adhesion work has been introduced.

It appears that the emulsification step can be controlled in a co-current disc and doughnut pulsed column (DDPC) in this unusual conditions compared to counter-current liquid–liquid extraction column. The DDPC is foreseen as a potential continuous tubular reactor for operations comprising an initial step of dispersion like in emulsion or suspension polymerization, crystallization processes and has demonstrated promising results in this approach.

References

[1] C. Gourdon, G. Casamata, Liquid Liquid Extraction Equipment, Godfrey and Slater, 1994.
[2] X. Ni, Y. Zhang, I. Mustafa, Correlation of polymer particle size with droplet size in suspension polymerization of methylmethacrylate in a batch oscillatory baffled reactor, Eng. Sci. Chem. 54 (1999) 841–850.
[3] A. Carvalho, D. Chicoma, C. Sayer, R. Giudici, Comparison of vinyl acetate butyl acrylate emulsion copolymerization conducted in a continuous pulsed sieve plate column reactor and in a batch stirred tank reactor, Macromol. Symp. 243 (2006) 147–158.
[4] I.-S. Stamenkovic, I.-B. Bankovic-Ilic, P.-B. Jovanic, V.-B. Veljkovic, D.-U. Skala, Hydrodynamics of a cocurrent upflow liquid–liquid reciprocating plate reactor for homogeneously base-catalyzed methanolysis of vegetable oils, Fuel 89 (2010) 3971–3984.
[5] R.-P. Borwankar, S.-I. Chung, D.-T. Wasan, Drop sizes in turbulent liquid-liquid dispersions containing polymeric suspension stabilizers. I. The breakage mechanism, J. Appl. Polym. Sci. 32 (1986) 5749–5762.
[6] K. Arai, M. Konno, Y. Matunaga, S. Saito, Effect of dispersed phase viscosity on the maximum stable drop size for breakup in turbulent flow, J. Chem. Eng. Jpn. 10 (1977) 325–330.
[7] E.-G. Chatzi, C. Kiparissides, Steady-state drop-size distributions in high holdup fraction dispersion systems, AIChE J. 41 (1995) 1640–1652.
[8] C. Kiparissides, G. Daskalakis, D.S. Achilias, Dynamic simulation of industrial poly(vinyl chloride) batch suspension polymerization reactors, Ind. Eng. Chem. Res. 36 (4) (1997) 1253–1267.

[9] C.-A. Angle, H.-A. Hamza, Predicting the sizes of toluene-diluted heavy oil emulsions in turbulent flow Part 2: Hinze-Kolmogorov based model adapted for increased oil fraction and energy dissipation in a stirred tank, Chem. Eng. Sci. 61 (2006) 7325–7335.
[10] G.-S. Calabrese, S. Pissavini, From batch to continuous flow processing in chemicals manufacturing, AIChE J. 57 (4) (2011) 828–834.
[11] M.-R. Mackley, X. Ni, Mixing and dispersion in a baffled tube for steady laminar and pulsatile flow, Chem. Eng. Sci. 46 (12) (1991) 3139–3151.
[12] M.-R. Mackley, X. Ni, Experimental fluid dispersion measurements in periodic baffled tube arrays, Chem. Eng. Sci. 48 (18) (1993) 3293–3305.
[13] M.-R. Mackley, K.-B. Smith, N.-P. Wise, The mixing and separation of particle suspensions using oscillatory flow in baffled tubes, Chem. Eng. Res. Des. 71 (A6) (1993) 649–656.
[14] G.-G. Stephens, M.-R. Mackley, Heat transfer performance for batch oscillatory flow mixing, Exp. Therm Fluid Sci. 25 (2002) 583–594.
[15] X. Ni, G. Brogan, A. Struthers, D.C. Bennett, S.-F. Wilson, A systematic study of the effect of geometrical parameters on mixing time in oscillatory baffled columns, Chem. Eng. Des. Res. Des. 76 (5) (1998) 635–642.
[16] A.-W. Fitch, J. Hongbing, X. Ni, An investigation of the effect of viscosity on mixing in an oscillatory baffled column using digital particle image velocimetry and computational fluid dynamics simulation, Chem. Eng. J. 112 (1–3) (2005) 197–210.
[17] X. Ni, Y. Zhang, I. Mustafa, Correlation of polymer particle size with droplet size in suspension polymerization of methylmethacrylate in a batch oscillatory baffled reactor, Chem. Sci. Eng. Sci. 54 (1999) 841–850.
[18] M.-J. Hounslow, X. Ni, Population balance modelling of droplet coalescence and break-up in an oscillatory baffled reactor, Chem. Eng. Sci. 59 (4) (2004) 819–828.
[19] N.-E. Pereira, X. Ni, Droplet size distribution in a continuous oscillatory baffled reactor, Chem. Eng. Sci. 56 (2001) 735–739.
[20] S. Lin, L.J. Chen, J.W. Wyu, W.J. Wang, An examination on the accuracy of interfacial tension measurement from pendant drop profiles, Langmuir 11 (1995) 4159–4166.
[21] T.-F. Tadros, B. Vincen, Encyclopedia of Emulsion Technology, vol. 1, Paul Bécher Edition, Marcel Dekker, New York, 1983.
[22] H.-W. Yarranton, J.-H. Masliyah, Numerical simulation of Ostwald Ripening in emulsions, J. Colloid Interface Sci. 196 (1997) 157–169.
[23] A.S. Kalbanov, K.N. Makarov, A.V. Pertzov, E.D. Shchukin, Ostwald ripening in emulsions, J. Colloid Interface Sci. 138 (1990) 98–104.
[24] J.-M.-G. Lankveld, J. Lyklema, Adsorption of polyvinyl alcohol on the paraffin-water interface III. Emulsification of paraffin in aqueous solutions of polyvinyl alcohol and the properties of paraffin-in-water emulsions stabilized by polyvinyl alcohol, J. Colloid Interface Sci. 41 (1972) 475–483.
[25] H. Nillson, C. Silvegren, B. Törnall, Suspension stabilizers fro PVC production I: Interfacial tension measurements, J. Vinyl Technol. 7 (1985) 112–118.
[26] Y. He, T. Howes, J.D. Lister, Dynamic Interfaical tension of aqueous solutions of PVAAs and its role in liquid-liquid dispersion stabilization, J. Chem. Eng. Jpn. 37 (2004) 181–186.
[27] G. Angelov, C. Gourdon, Pressure drop in pulsed extraction columns with internals of discs and doughnuts, Chem. Eng. Res. Des 90 (7) (2012) 897.
[28] P. Stonestreet, P.M.J. Van Der Veeken, The effects of oscillatory flow and bulk flow components on residence time distribution in baffled tube reactor, TransIChemE Part A 77 (1999) 671–684.
[29] M. Torab-Mostaedi, A. Ghaemi, M. Asadollahzadeh, Flooding and drop size in a pulsed disc and doughnut extraction column, Chem. Eng. Res. Des. 83 (2011) 2742–2751.
[30] K. Screenivasulu, D. Venkatanarasaiah, Y.-B.-G. Varma, Drop size distributions in liquid pulsed columns, Bioprocess Eng. 17 (1997) 189–195.
[31] N.E. Pereira. Characterisation of a continuous oscillatory baffle tubular reactor, PhD Thesis, Heriot-Watt University, Edinburgh, 2002.
[32] A. Kumar, S. Hartland, Prediction of dispersed phase holdup in pulsed perforated-plate extraction columns, Chem. Eng. Proc. 23 (1988) 41–59.
[33] A. Kumar, S. Hartland, Unified correlations for the prediction of drop size in liquid liquid extraction column, Ind. Eng. Res. Chem. Res. 35 (8) (1996) 2682–2685.
[34] A. Jahya, G.-W. Stevens, H.-R.-C. Pratt, Pulsed disc and doughnuts column performance, Solvent Extr. Ion Exchange 27 (1999) 63–82.
[35] I. Nahringbauer, Dynamic surface tension of aqueous polymer solution, I. Ethyl(hydroxyethyl) cellulose (BERMOCOLL cst-103), J. Colloid Interface Sci. 176 (1995) 318–328.
[36] M.-L. Van delden, N.-J.-M. Kuipers, A.-B. De Haan, Extraction of caprolactam with toluene in a pulsed disc and doughnut column-Part I: Recommandation of a model for hydraulic characteristics, Solvent Extr. Ion Exchange 24 (4) (2006).
[37] A.-C. Jealous, H.-F. Johnson, Power requirements for pulse Generation in Pulsed Columns, Ind. Eng. Chem. 47 (6) (1955) 1159–1166.
[38] M.-H.-I. Baird, P. Stonestreet, Energy dissipation in oscillatory flow within a baffled tube, Chem. Eng. Res. Des. 73 (A5) (1995) 503–511.
[39] M.S. Aoun Nabli, Simulation numérique de l'hydrodynamique et du mélange axial dans les colonnes d'extraction pulses à garnissage disques et couronnes, PhD thesis, INP Toulouse, 1995.
[40] F.B. Sprow, Distribution of drop sizes produced in turbulent liquid-liquid dispersion, Chem. Sci. Eng. 22 (1967) 435–442.
[41] J.O. Hinze, Fundamentals of the hydrodynamics mechanisms of splitting in dispersion process, AIChE J. 1 (1955) 289–295.
[42] C. Gourdon Les colonnes d'extraction par solvent: modèles et comportement, PhD thesis, INP Toulouse, 1989.
[43] Y. Liao, D. Lucas, A literature review on mechanisms and models for the coalescence process of fluid particles, Chem. Eng. Sci. 65 (2010) 2851–2864.
[44] A.-K. Chesters, The modelling of coalescence processes in fluid-liquid dispersions: a review of current understanding, Trans. IChemE Part A 69 (1991) 259–270.
[45] Y. Liao, D. Lucas, A literature review of theoretical models for drop and bubble breakup in turbulent dispersions, Chem. Eng. Sci. 64 (15) (2009) 3389–3406.
[46] S. Maass, M. Kraume, Determination of breakage rates using single drop experiments, Chem. Eng. Sci. 70 (2012) 146–164.
[47] C.A. Coulalouglou, L.-L. Tavlarides, Description of interaction processes in agitated liquid-liquid dispersion, Chem. Eng. Sci. 32 (11) (1977) 1289–1297.
[48] M.M. Ribeiro, P.F. Regueiras, M.M.L. Guimaraes, C.M.N. Madureira, J. Pinto, Optimization of breakage and coalescence model parameters in a steady-state batch agitated dispersion, Ind. Eng. Chem. Res. 50 (4) (2011) 2182–2191.
[49] A. Gäbler, M. Wegener, A. Paschedag, M. Kraume, The effect of pH on experimental and simulation results of transient drop size distributions in stirred liquid-liquid dispersions, Chem. Eng. Sci. 61 (9) (2006) 3018–3024.
[50] F. Azizi, A.M. Al Taweel, Turbulently flowing liquid–liquid dispersions. Part I: drop breakage and coalescence, Chem. Eng. J. 166 (2) (2011) 715–725.